Reaction mechanism and kinetics for Pt/CNTs catalyzed base-free oxidation of glycerol

Yuanyuan Ma[a,#], Jie Gan[a,#], Minjian Pan[a], Yanfang Zhang[a], Wenzhao Fu[a], Xuezhi Duan[a,*], Wenyao Chen[a], De Chen[b], Gang Qian[a,*], Xinggui Zhou[a]

[a] *State Key Laboratory of Chemical Engineering, East China University of Science and Technology, 130 Meilong Road, Shanghai 200237, China*

[b] *Department of Chemical Engineering, Norwegian University of Science and Technology, Trondheim 7491, Norway*

[#] These authors contributed equally to this work.

[*] Corresponding authors: xzduan@ecust.edu.cn; carlqg@ecust.edu.cn;

Tel.: +86-21-64250937; Fax.: +86-21-64253528

ABSTRACT: Fundamental understanding of heterogeneously catalyzed aerobic, base-free oxidation of glycerol is highly desirable for sustainable and highly efficient chemical synthesis. In this work, Pt/CNTs catalyzed base-free oxidation of glycerol is investigated by combining experiments, DFT calculations and kinetics analysis. The solvent effects and kinetic isotope effects measurements as well as DFT calculations reveal that water-assisted O_2 activation to form active OH* intermediates is not in rate-determining step (RDS) but in equilibrium. Then, Langmuir-Hinshelwood kinetic models are developed and fitted with the experimental data. The OH*-assisted C-H bond cleavage of glycerol is discriminated as the RDS for the two parallel oxidation pathways of glycerol via primary or secondary hydroxyl groups, where the former case exhibits lower activation energy. The insights revealed here could guide the design and optimization of this catalytic process to generate the targeted products.

Keywords: Base-free oxidation of glycerol; Solvent effects; DFT calculations; Kinetic isotope effects; Kinetics analysis

1. Introduction

Heterogeneously catalyzed aerobic, base-free oxidation of glycerol (GLY) to produce various value-added fine chemicals offers a simple, sustainable and environmentally benign alternative to traditional costly, multi-step and/or polluting base-promoted as well as stoichiometric oxidation processes (Bianchi et al., 2005; Zhou et al., 2008; Zope et al., 2010; Nie et al.,2012; Ning et al., 2015; Dodekatos et al., 2018a,b). For this process, a large amount of metal components (e.g., Pt, Pd and Au) and supports (e.g., carbon materials, oxide and zeolite) have been studied (Xu et al., 2008; Villa et al., 2010; Pestana et al., 2013; Wang et al., 2015; Shen et al., 2015; Xiao et al., 2016; Kaskow et al., 2018). Among them, conductive carbon materials, e.g., carbon nanotubes (CNTs), supported Pt catalysts have shown outstanding catalytic performance, which is mainly ascribed to the effective mass transfer and electron transfer of Pt with carbon support as well as low C-C cleavage of Pt catalyst (Liang et al., 2011; Lei et al., 2014; Zhang et al., 2015). Therefore, fundamental understanding of carbon supported Pt catalyzed base-free oxidation of glycerol is highly desirable for providing some controlling factors and mechanistic details, and then guiding the rational catalyst design and optimization.

For the carbon supported Pt catalyzed base-free oxidation of glycerol, there exists typical Pt size effects, and the optimal mean Pt particle size of 2~3 nm (Lei et al., 2014; Li and Zaera., 2015). Meanwhile, the remarkable Pt electronic effects have been also observed, and the catalyst with the higher Pt 4f binding energy is favorable for the reaction, while that with the lower Pt 4f binding energy is prone to be poisoned

by strongly adsorbed oxygen species (Lei et al., 2016). Moreover, DFT calculations have shown that the adsorption of oxygen atom from the primary hydroxyl group of glycerol on the Pt(111) surface is thermodynamically more stable than that of the secondary one, which is in accordance with the experimental observations of the preferential oxidation of the primary hydroxyl group (Duan et al., 2018). In principle, the oxidative dehydrogenation of the adsorbed glycerol most likely proceeds by means of either the resultant O* species from direct oxygen dissociation or the resultant OH* species from H_2O-assisted oxygen dissociation (Zope et al., 2010; Davis and Ide., 2014). However, it remains open for the preferred pathway of oxygen activation and the possible rate-determining step (RDS) of base-free glycerol oxidation.

The objective of this work is to fundamentally understand Pt/CNTs catalyzed base-free oxidation of glycerol from the mechanistic and kinetic points of view. The solvent effects and kinetic isotope effects experiments as well as DFT calculations were combined to probe whether and to what degree the water promotes the oxygen dissociation. Then, two Langmuir-Hinshelwood kinetic models were proposed and studied by assuming the first or second oxidative dehydrogenation step (O-H or C-H bond cleavage) being rate-determining step. Finally, the plausible rate-determining step was discriminated, and the kinetic parameters were obtained by fitting the model to the kinetic experimental data.

2 Experimental

2.1 Catalyst preparation and characterization

CNTs (Cnano (Zhen jiang) Technology Ltd.) with closed ends were used as received to prepare Pt catalyst with metal loading of 5 wt% by incipient wetness impregnation method. In brief, an aqueous solution of chloroplatinic acid (Sinopharm Chemical Reagent Co., Ltd.) was impregnated onto CNTs surfaces. The impregnated sample was dried in stagnant air at room temperature for 12 h followed by drying at 120 ºC for 12 h in an oven, and then reduced at 250 ºC for 2 h in a hydrogen flow (50 $cm^3 \cdot min^{-1}$). After being cooled to room temperature under Ar atmosphere, the reduced catalyst was passivated by 1% (v/v) O_2/Ar for 20 min. Moreover, transmission electron microscopy (TEM, JEOL JSM-1400, Japan) was employed to characterize the Pt/CNTs catalyst, and the Pt particle size distribution was determined by counting at least 200 random particles.

2.2 Catalyst testing

Unless otherwise stated, the glycerol oxidation reactions were performed at atmospheric pressure in a 250 mL four-neck flask equipped with a gas supply system, a mechanical stirrer, a condenser and a thermocouple. The flask was immersed in a well temperature-controlled water bath, where there is no obvious reaction temperature change during the whole reaction process. Generally, appropriate amounts of glycerol aqueous solution and Pt/CNTs catalysts were added into the reactor with desired stirring speed. Once the required temperature was reached, O_2 or

O_2/N_2 mixed gas was bubbled into reactor via a mass flow controller.

In order to estimate the influence of external mass transfer limitations, the oxidation experiments were respectively carried out using different stirring speeds, oxygen flow rates and GLY/Pt molar ratios with other conditions constant, i.e., 160 mL aqueous solution of glycerol (0.1 g/mL) and 60 ºC. By excluding the effects of transport limitations, the kinetic experiments were performed at atmospheric pressure with varied initial glycerol concentration, oxygen partial pressure and reaction temperature. All experiments were repeated at least three times with a relative error of less than 2% among the repeated measurements. Furthermore, the oxidation experiments were also conducted using absolute ethanol or D_2O instead of H_2O as solvent to investigate the role of water in base-free oxidation of glycerol. The other reaction conditions are as following: 30 mL glycerol solution (0.1 g/mL), GLY/Pt molar ratio of 4000, pure oxygen with flow rate of 150 $cm^3 \cdot min^{-1}$, 60 ºC and 1000 rpm.

2.3 Products analysis

During the reaction, the samples were removed periodically and filtered using 0.22 μm NY filters before analysis with a high performance liquid chromatograph (HPLC, Agilent 1100). The HPLC was equipped with refractive index and UV detectors using a BP-OA column (300×7.8 mm) operating at 80 ºC. Diluted H_3PO_4 (0.001 $g \cdot mL^{-1}$) operating at 0.5 $mL \cdot min^{-1}$ was employed as eluent. The retention time and calibration curves for observed products were determined by injecting the standard samples.

2.4 Computational details

Density functional theory (DFT) calculations of oxygen activation on Pt(111) were performed using the Vienna ab initio simulation package (VASP) (Kresse and Hafner., 1993; Kresse and Furthmüller., 1996a,b; Kresse et al., 1994). The Pt(111) surface was modelled using a p(3×3) supercell slab model, containing four atomic layer slabs with a relaxation of the top two layers, and a vacuum thickness of 12 Å was used to avoid the interaction from the top supercells. The ion-electron interaction was described with the projector augmented wave (PAW) method (Blöchl, 1994), and the electron exchange-correlation was GGA-PBE (Kresse and Joubert., 1999; Perdew et al., 1996). The Dimer method was used to determine the transition states of the elementary steps (Henkelman and Jónsson., 2000). The Hellman-Feynman force on each ion was minimized to be less than 0.03 eV/Å. Notably, exemplified with the two crucial elementary steps, i.e., direct O_2 dissociation and water-assisted O_2 dissociation, testing of the effects of Monkhorst-Pack k-point mesh (Monkhorst and Pack., 1976; Methfessel and Paxton., 1989) and cutoff energy in Table S1 shows slight differences in those calculated results, and the 5 × 5× 1 k point and the cutoff energy of 450 eV are accurate enough to calculate the oxygen activation.

3 Results and discussion

3.1 Solvent effects and kinetic isotope effects

One typical Pt/CNTs catalyst with the Pt loading of 5 wt% was prepared and characterized by TEM, which exhibits average Pt particle size of 2.0 nm in Fig. 1a.

Such catalyst was employed to comparatively study the solvent effects on the base-free oxidation of glycerol with oxygen in aqueous or ethanol solution, and then to probe whether and to what degree water plays a crucial role in the reaction. It is noted that the absolute ethanol as the referenced solvent well mixes with glycerol and has higher oxygen solubility than the water (Dodekatos et al., 2018b), and no additional side reactions, i.e., absolute ethanol oxidation over the same Pt/CNTs catalyst under the reaction conditions, are observed according to preliminary experimental results. It can be obviously seen in Fig. 1b that using ethanol as the solvent gives rise to an unexpected lower glycerol conversion than using water as the solvent despite the former one with the improved oxygen solubility. This suggests remarkable solvent effects on the reaction.

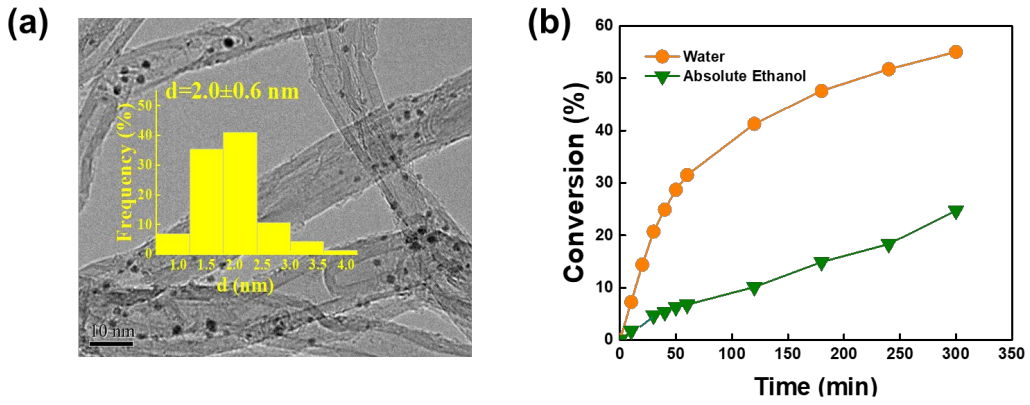

Fig. 1 (a) Typical TEM image and the corresponding particle size distribution of Pt/CNTs catalyst, and (b) glycerol conversion as a function of time over Pt/CNTs catalysts in water and absolute ethanol. Reaction conditions: $C_{GLY,0}$=0.1 g/mL, m_{GLY}=3 g, T=60 °C, P_{O2}=1 bar, n_{GLY}/n_{Pt}=850, stirring speed=1000 rpm.

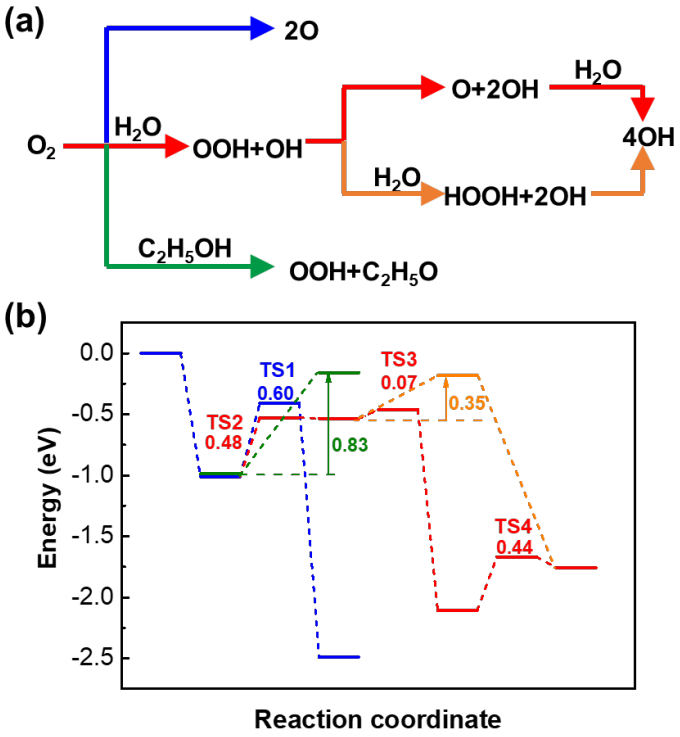

Fig. 2 (a) The reaction pathways and (b) the corresponding relative energy profile for direct O_2 dissociation (blue), H_2O-assisted one (red and orange) and ethanol-assisted one (green) pathways, respectively.

To understand the solvent effects, we resort to DFT calculations for comparing the effects of the solvents on the O_2 activation by means of direct O_2 dissociation, H_2O-assisted one and/or ethanol-assisted one, as schematically shown in Fig. 2a. It can be clearly observed in Fig. 2b that for the point of thermodynamic view, the ethanol-assisted O_2 dissociation is highly exothermic than the H_2O-assisted one, while the direct O_2 dissociation is highly endothermic; the first activation step in the H_2O-assisted O_2 dissociation pathway exhibits activation energy of 0.48 eV, which is lower than the direct O_2 dissociation (i.e., 0.60 eV). These results indicate the promotional effects of the water solvent on the O_2 activation in comparison to the ethanol solvent, and the most likely occurrence of the direct O_2 activation in the

ethanol solvent when combining to the results of Fig. 1b. In addition, the H_2O-assisted O_2 dissociation is also observed to proceed via the OOH* cleavage rather than the HOOH* intermediate to form active OH* species. Notably, in previous studies, O_2 activation has been found to be highly sensitive to the types of reactions (e.g., ORR, alcohol oxidation) and catalysts (e.g., Au, Pd, Pt) as well as the water content (Ou et al., 2009; Chang et al., 2013; Hibbitts and Neurock, 2013; Tran et al., 2016). Bearing this in mind, kinetic isotope effects (KIE) measurements were further carried out below to probe whether the H_2O-assisted O_2 activation is in rate-determining step (RDS) for the glycerol oxidation or in equilibrium. This is because it is very crucial to establish the kinetics models in the following Section 3.2.

Along this line, H/D kinetic isotope effects for the Pt/CNTs catalyzed base-free oxidation of glycerol were explored, and the results are shown in Fig.3. From the slopes of the curves in the initial reaction period, the initial reaction rates of glycerol oxidation using H_2O or D_2O as the reactant are respectively determined to be 370 and 288 $mol_{GLY}\cdot h^{-1}\cdot mol_{Pt}^{-1}$, and thus a value of $k_H/k_D \approx 1.3$ is obtained. Generally, a small KIE value of 0.7-1.5 implies that no bond to the isotopically substituted atom in the reactant is broken or formed in RDS (Westaway., 2007; Chen et al., 2016; Chen et al., 2017; Li et al., 2017). Therefore, the small KIE value here suggests that the H_2O-assisted O_2 activation is rate relevant, but not in RDS. In other words, the relevant steps concerning the O-H bond cleavage of water proceed before the RDS, and can be assumed to be in equilibrium as follows:

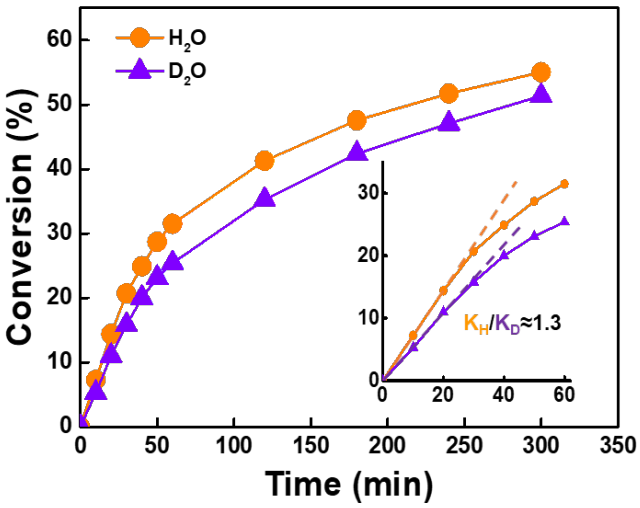

Fig. 3 Glycerol conversion as a function of time over Pt/CNTs catalysts in H_2O and D_2O. Reaction conditions: $C_{GLY,0}$=0.1 g/mL, m_{GLY}=3 g, T=60 °C, P_{O2}=1 bar, n_{GLY}/n_{Pt}=850, stirring speed=1000 rpm.

$$H_2O + * \rightleftharpoons H_2O* \quad (1)$$

$$O_2 + * \rightleftharpoons O_2* \quad (2)$$

$$O_2* + H_2O* \rightarrow OOH* + OH* \quad (3)$$

$$OOH* + * \rightarrow O* + OH* \quad (4)$$

$$O* + H_2O* \rightarrow OH* + OH* \quad (5)$$

The equations (3)-(5) can be combined as:

$$O_2* + 2H_2O* + * \rightleftharpoons 4OH* \quad (6)$$

3.2 Reaction kinetics

As mentioned above, for Pt/CNTs catalyzed base-free oxidation of glycerol, water can promote oxygen dissociation to form OH* species, and the resultant OH* species on Pt surface might facilitate the O-H bond activation of adsorbed glycerol and the

subsequent activation of C-H bond to form glyceraldehyde (GLYD) and dihydroxyacetone (DHA), as schematically shown in Scheme 1. For this process, it is still unknown which step, the first or second dehydrogenation of glycerol (the O-H or C-H bond cleavage step), is in RDS, and whether the mechanisms for the oxidation of the primary hydroxyl group to GLYD (Route 1) and that of the secondary one to DHA (Route 2) are similar. Therefore, a detailed kinetic analysis is performed aiming to provide some insights into the reaction mechanism.

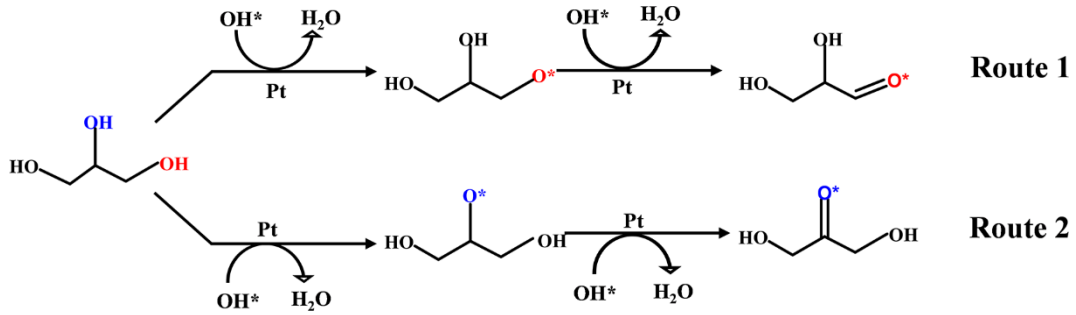

Scheme 1 Possible mechanism for initial oxidative dehydrogenation of glycerol under base-free conditions over Pt-based catalyst.

By assuming the O-H or C-H bond cleavage of glycerol being in RDS, two models can be created, respectively. Only the main compounds, GLYD and its oxidation product glyceric acid (GLYA), and DHA are taken into account as the kinetic experiments were performed at low glycerol conversion (~10%). Moreover, since there is no reaction without catalysts, only surface species are involved in the reactions.

Model 1:

Besides the steps of water and oxygen adsorption and OH* species generation (Eqs. 1, 2 and 6), the following main steps are also assumed to occur on the surface of Pt:

The adsorption of glycerol：

$$CH_2OHCHOHCH_2OH + * \overset{k_4}{\underset{k_{-4}}{\rightleftharpoons}} CH_2OHCHOHCH_2OH* \quad (7)$$

the first dehydrogenation of adsorbed glycerol, i.e., the cleavage of the primary and the secondary hydroxyl group with the assistance of adsorbed OH*, considered as the RDS：

$$CH_2OHCHOHCH_2OH* + OH* \overset{k_5}{\rightleftharpoons} CH_2OHCHOHCH_2O* + H_2O* \quad (8)$$

$$CH_2OHCHOHCH_2OH* + OH* \xrightarrow{k_6} CH_2OHCHOCH_2OH* + H_2O* \quad (9)$$

In this model, the steps occurring after the RDS are not considered. Therefore, the coverage of each reactant species and OH* species may be derived, in which $K_i=k_i/k_{-i}$:

$$\theta_{H_2O} = K_1 C_{H_2O} \theta_V \quad (10)$$

$$\theta_{O_2} = K_2 P_{O_2} \theta_V \quad (11)$$

$$\theta_{OH} = (K_3 \theta_{O_2} \theta_{H_2O}^2 \theta_V)^{0.25} \quad (12)$$

$$\theta_{GLY} = K_4 C_{GLY} \theta_V \quad (13)$$

According to a Langmuir-Hinshelwood-type reaction, the corresponding rates of steps 8 and 9 can be written as follows:

$$r_5 = k_5 q_{GLY} q_{OH} \quad (14)$$

$$r_6 = k_6 q_{GLY} q_{OH} \quad (15)$$

By combining $\theta_{O_2} + \theta_{H_2O} + \theta_{GLY} + \theta_{OH} + \theta_V = 1$ with Eqs.10-13, the rate expressions can be derived as:

$$r_5 = \frac{k_5 K_4 (K_1^2 K_2 K_3)^{0.25} P_{O_2}^{0.25} C_{GLY}}{[K_4 C_{GLY} + K_1 + K_2 P_{O_2} + (K_1^2 K_2 K_3 P_{O_2})^{0.25} + 1]^2} \quad (16)$$

$$r_6 = \frac{k_6 K_4 (K_1^2 K_2 K_3)^{0.25} P_{O_2}^{0.25} C_{GLY}}{[K_4 C_{GLY} + K_1 + K_2 P_{O_2} + (K_1^2 K_2 K_3 P_{O_2})^{0.25} + 1]^2} \quad (17)$$

The mass balance equations for the main compounds in the system can then be given by:

$$\frac{1}{W}\frac{dC_{GLY}}{dt} = -r_5 - r_6 \quad (18)$$

$$\frac{1}{W}\frac{d(C_{GLYD} + C_{GLYA})}{dt} = r_5 \quad (19)$$

$$\frac{1}{W}\frac{dC_{DHA}}{dt} = r_6 \quad (20)$$

Model 2:

The steps of reactant species adsorption and OH* species generation are the same as those in Model 1, but the second dehydrogenation steps with the assistance of adsorbed OH* are considered as in RDS, and thus the first dehydrogenation steps are assumed to be in equilibrium：

The first dehydrogenation step of glycerol：

$$CH_2OHCHOHCH_2OH* + OH* \overset{k_5}{\underset{k_{-5}}{\rightleftharpoons}} CH_2OHCHOHCH_2O* + H_2O* \quad (21)$$

$$CH_2OHCHOHCH_2OH* + OH* \overset{k_6}{\underset{k_{-6}}{\rightleftharpoons}} CH_2OHCHOCH_2OH* + H_2O* \quad (22)$$

The second dehydrogenation step of glycerol：

$$CH_2OHCHOHCH_2O* + OH* \xrightarrow{k_7} CH_2OHCHOHCHO* + H_2O* \quad (23)$$

$$CH_2OHCHOCH_2OH* + OH* \xrightarrow{k_8} CH_2OHCOCH_2OH* + H_2O* \quad (24)$$

Similarly, the rate expressions of steps 23 and 24 can be derived as:

$$r_{20} = \frac{k_7 K_4 K_5 (K_2 K_3 P_{O_2})^{0.5} C_{GLY}}{[K_4 C_{GLY} + K_1 C_{H_2O} + K_2 P_{O_2} + (K_1^2 K_2 K_3 P_{O_2} C_{H_2O}^2)^{0.25} + (K_5 + K_6)\frac{K_4 C_{GLY} (K_2 K_3 P_{O_2})^{0.25}}{K_1^{0.5} C_{H_2O}^{0.5}} + 1]^2} \quad (25)$$

$$r_{21} = \frac{k_8 K_4 K_6 (K_2 K_3 P_{O_2})^{0.5} C_{GLY}}{[K_4 C_{GLY} + K_1 C_{H_2O} + K_2 P_{O_2} + (K_1^2 K_2 K_3 P_{O_2} C_{H_2O}^2)^{0.25} + (K_5 + K_6)\frac{K_4 C_{GLY} (K_2 K_3 P_{O_2})^{0.25}}{K_1^{0.5} C_{H_2O}^{0.5}} + 1]^2} \quad (26)$$

By setting $K_1' = K_1 C_{H_2O}$, $K_3' = (K_1^2 K_2 K_3 C_{H_2O}^2)^{0.25}$, $K_5' = (K_5 + K_6)\frac{K_4 (K_2 K_3)^{0.25}}{K_1^{0.5} C_{H_2O}^{0.5}}$, $K_7' = k_7 K_4 K_5 (K_2 K_3)^{0.5}$ and $K_8' = k_8 K_4 K_6 (K_2 K_3)^{0.5}$, the rate expressions can be

rewritten as follows:

$$r_{20} = \frac{K'_7 C_{GLY} P_{O_2}{}^{0.5}}{[K_4 C_{GLY} + K'_1 + K_2 P_{O_2} + K'_3 P_{O_2}{}^{0.25} + K'_5 C_{GLY} P_{O_2}{}^{0.25} + 1]^2} \quad (27)$$

$$r_{21} = \frac{K'_8 C_{GLY} P_{O_2}{}^{0.5}}{[K_4 C_{GLY} + K'_1 + K_2 P_{O_2} + K'_3 P_{O_2}{}^{0.25} + K'_5 C_{GLY} P_{O_2}{}^{0.25} + 1]^2} \quad (28)$$

Similarly, the mass balance equations for the main compounds in the system can then be given by:

$$\frac{1}{W}\frac{dC_{GLY}}{dt} = - r_{20} - r_{21} \quad (29)$$

$$\frac{1}{W}\frac{d(C_{GLYD} + C_{GLYA})}{dt} = r_{20} \quad (30)$$

$$\frac{1}{W}\frac{dC_{DHA}}{dt} = r_{21} \quad (31)$$

It can be noted that the big difference between the two models lies in the reaction order. The maximum order with respect to oxygen pressure is 0.25 for Model 1 and 0.50 for Model 2, respectively, although those with respect to glycerol concentration are 1.0 for both models.

In order to determine the reaction orders in glycerol and oxygen, kinetic experiments were performed at atmospheric pressure with varied initial glycerol concentration and oxygen partial pressure. To ensure the reaction kinetics measured in the absence of mass transfer limitations, several groups of experiments were first carried out by varying stirring speed, oxygen flow rate and catalyst amount. As shown in Fig. 4, at a stirring speed of 300 rpm, the initial glycerol conversion is lower than those at other stirring speeds, which may be due to the external mass transport resistance. By increasing the speed from 700 to 1000 rpm, no substantial changes in initial conversion are observed, suggesting the elimination of external mass transfer

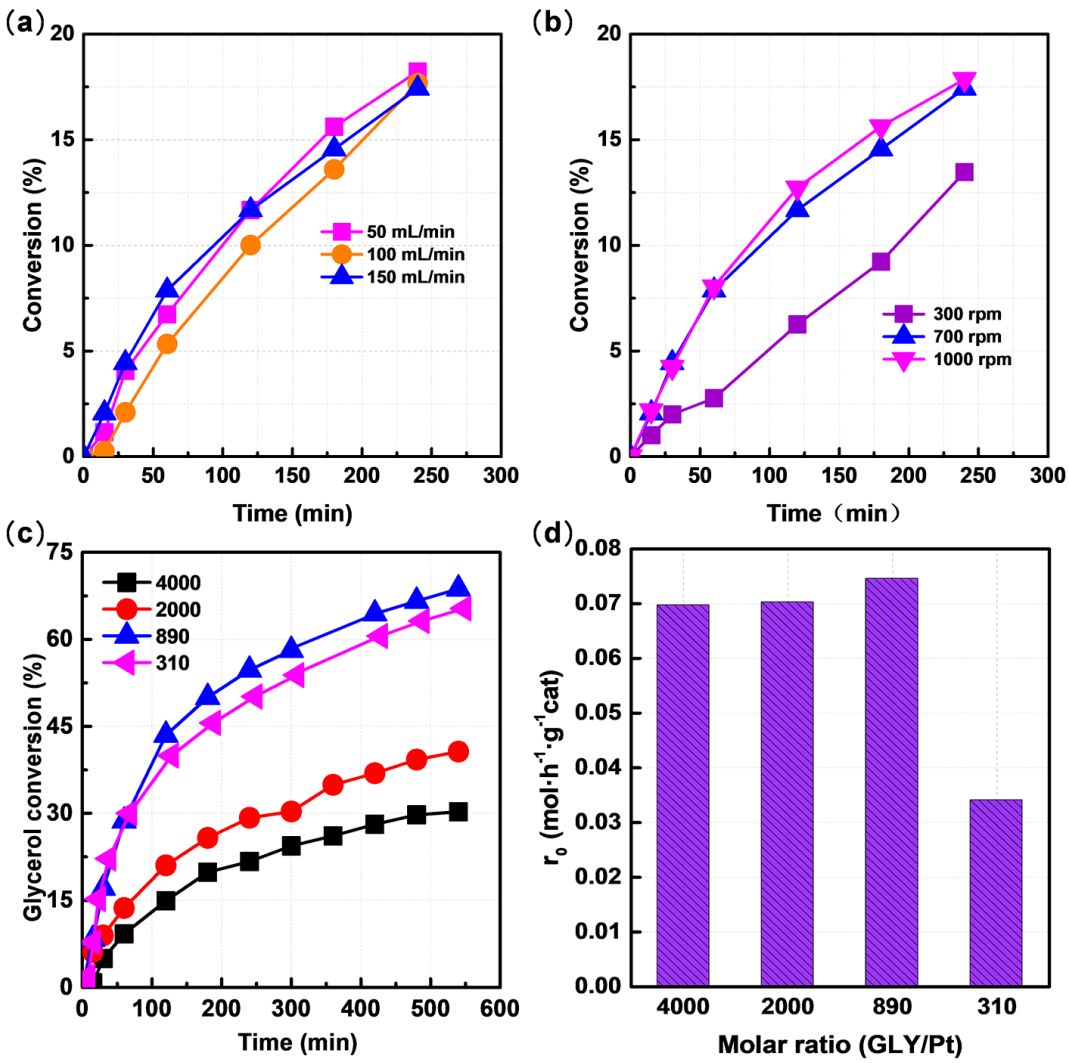

Fig. 4 Glycerol conversion as a function of time over Pt/CNTs catalysts with different (a) Oxygen flow rates, (b) Stirring speeds, and (c) GLY/Pt molar ratios, and (d) The effects of GLY/Pt molar ratio on the initial reaction rate. Other reaction conditions: $C_{GLY,0}$=0.1 g/mL, T=60 ºC, P_{O2}=1 bar.

limitations. Similarly, the initial glycerol conversion appeared to be independent of the oxygen flow rate varying from 50 to 150 $cm^3 \cdot min^{-1}$ and the initial reaction rate remains nearly constant with the GLY/Pt molar ratio in the range of 890-4000 indicating that the reaction proceeds under kinetic regime environment. Moreover, the effects of internal mass transfer limitations can be ignored based on the unique pore

characteristics of CNTs we have reported (Duan et al., 2018). Therefore, in the kinetic experiments, the conditions of 700 rpm, 150 $cm^3 \cdot min^{-1}$ and GLY/Pt molar ratio of 4000 were employed, and the evaluation of the kinetic model was made with the experimental results obtained at low glycerol conversion (<10%).

On the basis of the kinetic data from the reaction took place under varied initial glycerol concentrations and oxygen partial pressure conditions, the initial formation rates of the products from the oxidation of the primary (Route 1) and the secondary hydroxyl group (Route 2) were respectively calculated, and the method of initial rates was then used to determine the reaction order. By assuming the rate law in the form of $r_0 = kC_{GLY,0}^{\alpha} p_{O_2}^{\beta}$, the slopes of the plots of $\ln r_0$ versus $\ln C_{GLY,0}$ and $\ln r_0$ versus $\ln p_{O2}$ will give the reaction orders with respect to glycerol concentration (α) and oxygen partial pressure (β), respectively.

Fig. 5a shows the plot of $\ln r_0$ versus $\ln C_{GLY,0}$, which indicates that both the initial formation rates of the products from the two routes are almost constant in the studied glycerol concentration. In other words, with respect to glycerol concentration, the reaction orders of the products from the two routes can be both considered as zero. Similarly, $\ln r_0$ versus $\ln p_{O2}$ for the two routes are plotted in Fig. 5b. The two plots are linear with a slope of 0.52±0.02, and 0.30±0.02, respectively. This means that with respect to oxygen partial pressure, the reaction order of the products from the oxidation of the primary hydroxyl group is about 0.5, while that for the oxidation of the secondary one is about 0.3. The obtained reaction orders, which are both larger than 0.25, but smaller than or equal to 0.5, indicate that Model 2 may be more suitable

to describe the possible reaction mechanism than Model 1, i.e., the secondary dehydrogenation of glycerol (C-H bond cleavage) with the assistance of adsorbed OH* being in RDS. This also indicates that the two parallel oxidation pathways of glycerol via primary or secondary hydroxyl groups have similar reaction mechanism.

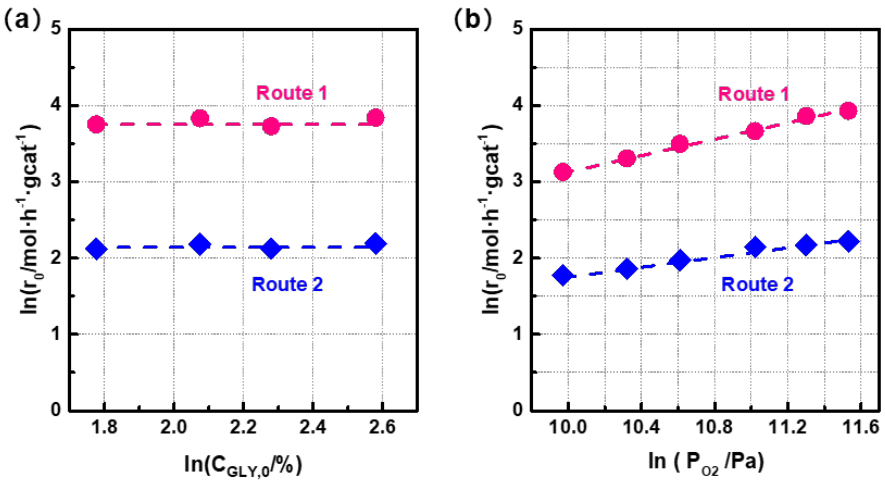

Fig. 5. The effects of (a) initial glycerol concentration and (b) oxygen pressure on the oxidation of the primary (Route 1) and the secondary hydroxyl group (Route 2). Reaction conditions: 160 mL of glycerol aqueous solution, n_{GLY}/n_{Pt} = 4000, T=60 °C, stirring speed=700 rpm.

A series of experiments with transport limitations excluded were then carried out at different temperatures (40, 50, 60 and 70 °C) to determine kinetic parameters. The total concentration of GLYD and GLYA from route 1 and that of DHA from route 2 at low conversion (<10%) were obtained and exhibited in Fig. 6. Under low glycerol conversion, product concentrations from both routes increase linearly with an increase in reaction time. Model 2 was employed to fit the experimental data. The model was solved using the Matlab ode15s subroutine to obtain the concentration profiles as a function of time. The kinetic parameters were then estimated by the non-linear fitting

using the subroutine lsqcurvefit by minimizing the objective function, the sum of square error (SQE) defined as $SQE = \sum_i (C_i^{\exp} - C_i^{cal})^2$, where $C_i^{\exp}$ and C_i^{cal} are the experimental and the calculated concentration, respectively. As shown in Fig. 7, the calculated results are in good agreement with the experimental data, indicating that Model 2 can give a good description for the reaction.

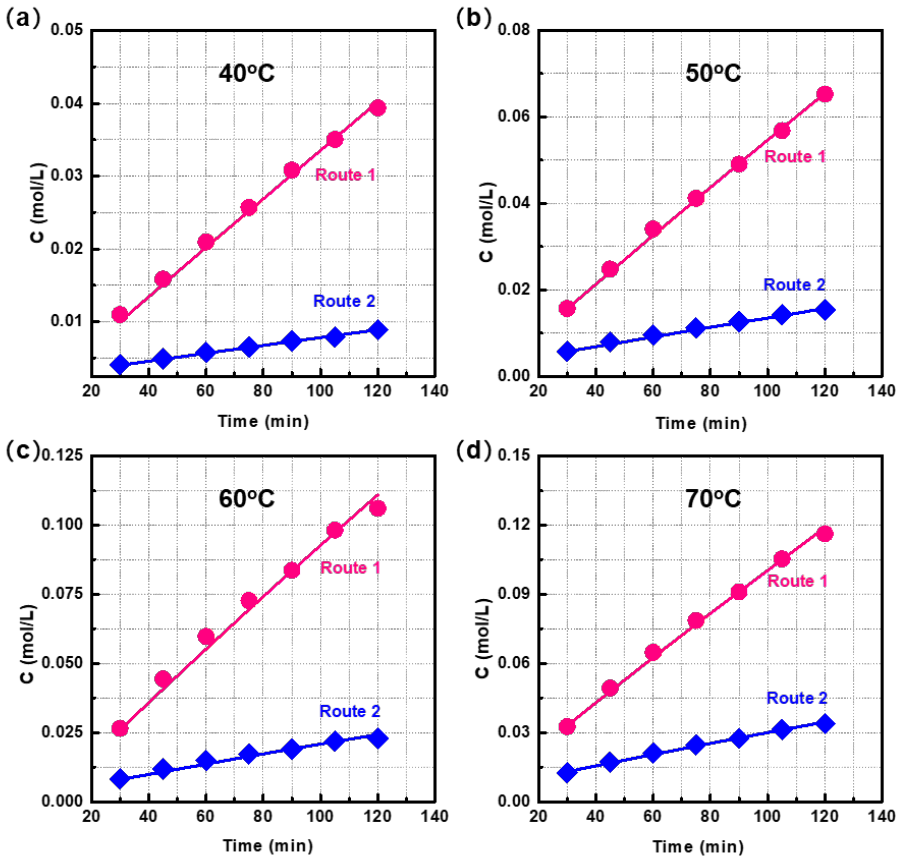

Fig. 6 Comparison of the experimental and calculated concentration of the product from the oxidation of the primary (Route 1) and the secondary hydroxyl group (Route 2) (dots: experimental data, lines: calculated data). Reaction conditions: 160 mL of glycerol aqueous solution, $C_{GLY,0}$=0.1 g/mL, T=60 °C, P_{O2}=1 bar, n_{GLY}/n_{Pt} =4000, stirring speed=700 rpm.

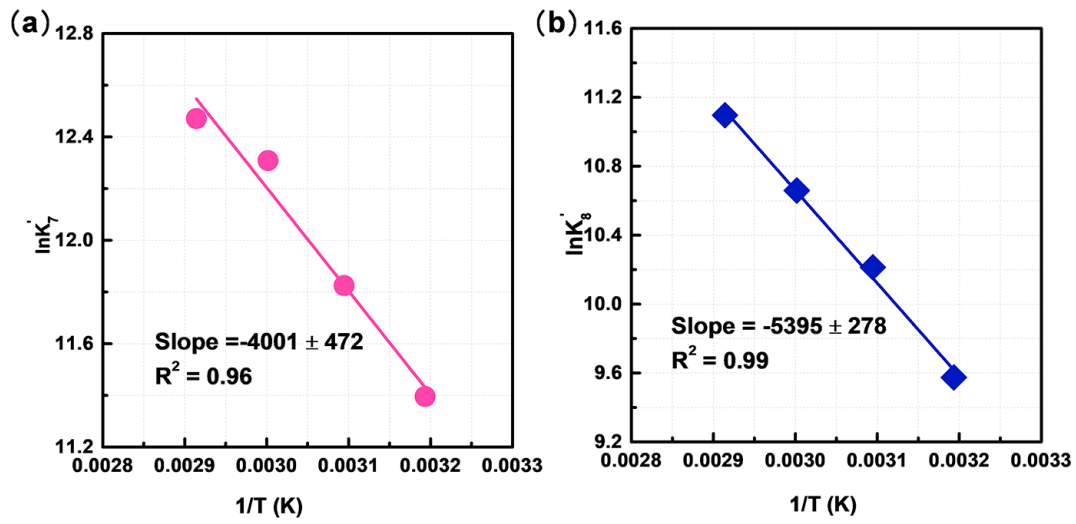

Fig. 7 Arrhenius-type plot for the oxidation of (a) the primary and (b) the secondary hydroxyl group of glycerol.

Based on the estimated parameters listed in Table 1, the Arrhenius plots of $\ln K_7'$ and $\ln K_8'$ against 1/T were respectively developed, and two straight lines with the correlation coefficients of 0.99 and 0.96 were obtained. From the slopes of the two lines, the activation energy (E_a) over the two reaction routes can be estimated as 33.3±3.9 and 44.9±2.3 kJ/mol, respectively. Apparently, the oxidation of the primary hydroxyl group (Route 1) has a lower activation energy than that of the secondary one (Route 2), suggesting that at low temperature more products from the oxidation of primary hydroxyl group could be obtained.

Table 1 Results of kinetic parameters estimation

T (°C)	K_1	K_2'	K_3	K_4'	K_5'	K_7'	K_8'
40	9.8E-04	1.80E+03	3.0E-04	1.48E-01	2.6E-10	8.89E+04	1.44E+04
50	7.7E-04	1.71E+03	2.6E-04	9.43E-01	5.0E-08	1.37E+05	2.73E+04
60	6.5E-04	1.61E+03	1.0E-04	3.25E+00	2.9E-08	2.22E+05	4.26E+04
70	6.0E-04	1.52E+03	9.90E-05	1.37E+01	2.4E-05	2.61E+05	6.59E+04

4. Conclusions

In summary, we have revealed the reaction mechanism of Pt/CNTs catalyzed base-free oxidation of glycerol by combining the solvent effects measurements, DFT calculations and kinetic (isotopic) analyses. The water-assisted O_2 dissociation to form active OH* intermediate has been demonstrated to be not in RDS but in equilibrium, and the OH*-assisted C-H bond cleavage of glycerol to be in RDS for the two parallel oxidation pathways of glycerol via primary or secondary hydroxyl groups. The glycerol oxidation favorably proceeds via the primary hydroxyl group than the secondary one. These results demonstrated here could be valuable to guide the rational design and optimization of Pt-based catalysts for base-free oxidation of glycerol, such as tailoring the Pt geometric and electronic properties with promoters or changing the support surface chemistry to promote the water-assisted O_2 dissociation and then aim to enhance the OH*-assisted C-H bond cleavage to generate more targeted product.

Declaration of interest

The authors declare no conflict of interest.

Acknowledgments

This work was financially supported by the Natural Science Foundation of China (21776077), the Shanghai Natural Science Foundation (17ZR1407300 and 17ZR1407500), the Program for Professor of Special Appointment (Eastern Scholar)

at Shanghai Institutions of Higher Learning, the Shanghai Rising-Star Program (17QA1401200), the Open Project of State Key Laboratory of Chemical Engineering (SKLChe-15C03), the State Key Laboratory of Organic-Inorganic Composites (oic-201801007), the Fundamental Research Funds for the Central Universities (222201718003), and the 111 Project of the Ministry of Education of China (B08021).

Nomenclature

CNTs	carbon nanotubes
DFT	density functional theory
DHA	dihydroxyacetone
GLY	glycerol
GLYA	glyceric acid
GLYD	glyceraldehyde
KIE	kinetic isotope effects
RDS	rate-determining step
C_i	concentration of i, mol L^{-1}
Ki	equilibrium constant
ki	rate constant
n_i	number of particles
r_i	reaction rate, mmol h^{-1} $gcat^{-1}$
P	pressure, Pa
W	mol surface Pt per liter solution
Ea	activation energy, kJ mol^{-1}
θ_i	surface coverage of species i

Literature Cited

Bianchi, C.L., Canton, P., Dimitratos, N., Porta, F., Prati, L., 2005. Selective oxidation of glycerol with oxygen using mono and bimetallic catalysts based on Au, Pd and Pt metals. Catal. Today. 102, 203-212.

Blöchl, P.E., 1994. Projector augmented-wave method. Phys. Rev. B. 50, 17953.

Chang, C.R., Yang, X.F., Long, B., Li, J., 2013. A water-promoted mechanism of alcohol oxidation on a Au(111) surface: Understanding the catalytic behavior of bulk gold. ACS Catal. 3, 1693-1699.

Chen, W.Y., Li, D.L., Peng, C., Qian, G., Duan, X.Z., Chen, D., Zhou, X.G., 2017. Mechanistic and kinetic insights into the Pt-Ru synergy during hydrogen generation from ammonia borane over PtRu/CNT nanocatalysts. J. Catal. 356, 186-196.

Chen, W.Y., Li, D.L., Wang, Z.J., Qian, G., Sui, Z.J., Duan, X.Z., Zhou, X.G., 2016. Reaction mechanism and kinetics for hydrolytic dehydrogenation of ammonia borane on a Pt/CNT catalyst. AIChE J. 63, 60-65.

Davis, R.J., Ide, M.S., 2014. The important role of hydroxyl on oxidation catalysis by gold nanoparticles. Accounts. Chem. Res. 47, 825-833.

Dodekatos, G., Schünemann, S., Tüysüz, H., 2018a. Recent advances in thermo-, photo-, and electrocatalytic glycerol oxidation. ACS Catal. 8, 6301-6333.

Dodekatos, G., Temieden, J., Schünemann, S., Weidenthaler, C., Tüysüz, H., 2018b. Promoting effect of solvent on Cu/CoO catalyst for selective glycerol oxidation under alkaline conditions. Catal. Sci. Technol. 8, 4891-4899.

Duan, X.Z., Zhang, Y.F., Pan, M.J., Dong, H., Chen, B.X., Ma, Y.Y., Qian, G., Zhou, X.G., Yang, J., Chen, D., 2018. SbOx-promoted Pt nanoparticles supported on CNTs as catalysts for base-free oxidation of glycerol to dihydroxyacetone. AIChE J. 64, 3979-3987.

Hibbitts, D, D., Neurock, M., 2013. Influence of oxygen and pH on the selective oxidation of ethanol on Pd catalysts. J Catal. 299, 261-271.

Henkelman, G., Jónsson, H., 2000. Improved tangent estimate in the nudged elastic band method for finding minimum energy paths and saddle points. J. Chem. Phys.113, 9978-9985.

Kaskow, I., Decyk, P., Sobczak, I., 2018. The effect of copper and silver on the properties of Au-ZnO catalyst and its activity in glycerol oxidation. Appl. Surf. Sci. 444, 197-207.

Kresse, G., Hafner, J., 1993. Ab initio molecular dynamics for liquid metals. Phys. Rev. B. 47, 558 .

Kresse, G., Furthmüller, J., Hafner, J., 1994. Theory of the crystal structures of selenium and tellurium: The effect of generalized-gradient corrections to the local-density approximation. Phys. Rev. B. Condens. Matter. Mater. Phys. 50, 13181-13185.

Kresse, G., Furthmüller, J., 1996a. Efficiency of ab initio total energy calculations for metals and semiconductors using a plane-wave basis set. Comp. Mater. Sci. 6, 15-50.

Kresse, G., Furthmüller, J., 1996b. Efficient iterative schemes for ab initio total

energy calculations using a plane-wave basis set. Phys. Rev. B. 54, 11169.

Kresse, G., Joubert, D., 1999. From ultrasoft pseudopotentials to the projecter augmented-wave method. Phys. Rev. B. 59, 1758-1775.

Lei, J.Q., Duan. X.Z., Qian, G., Chen, D., Zhou, X.G., 2014. Size effects of Pt nanoparticles supported on carbon nanotubes for selective oxidation of glycerol in a base-free condition. Ind. Eng. Chem. Res. 53, 16309-16315.

Lei, J.Q., Dong. H., Duan. X.Z., Chen, W.Y., Qian, G., Chen, D., Zhou, X.G., 2016. Insights into activated carbon-supported platinum catalysts for base-free oxidation of glycerol. Ind. Eng. Chem. Res. 55, 420-427.

Li, Y., Zaera, F., 2015. Sensitivity of the glycerol oxidation reaction to the size and shape of the platinum nanoparticles in Pt/SiO_2 catalysts. J. Catal. 326, 116-126.

Li, Z., He, T., Liu, L., Chen, W.D., Zhang, M., Wu, G.T., Chen, P., 2016. Covalent triazine framework supported non-noble metal nanoparticles with superior activity for catalytic hydrolysis of ammonia borane: from mechanistic study to catalyst design. Chem. Sci. 8, 781-788.

Liang, D., Gao, J., Chen, P., Wei, Y., Hou, Z.Y., 2011. Bimetallic Pt-Cu catalysts for glycerol oxidation with oxygen in a base-free aqueous solution. Catal. Commun. 12, 1059-1062.

Methfessel, M., Paxton, A.T., 1989. High-precision sampling for Brillouin-zone integration in metals. Phys. Rev. B. 40, 3616.

Monkhorst, H.J., Pack, J.D., 1976. Special points for Brillouin-zone integrations. Phys. Rev. B. 13, 5188.

Nie, R.F., Liang, D., Shen, L., Gao, J., Chen, P., Hou, Z.Y., 2012. Selective oxidation of glycerol with oxygen in base-free solution over MWCNTs supported PtSb alloy nanoparticles. Appl. Catal. B-Environ. 127, 212-220.

Ning, X.M., Li, Y.H., Yu, H., Peng, F., Wang, H.J., Yang, Y.H., 2015. Promoting role of bismuth and antimony on Pt catalysts for the selective oxidation of glycerol to dihydroxyacetone. J. Catal. 335, 95-104.

Ou L., Yang F., Liu Y., Chen S L., 2009. First-principle study of the adsorption and dissociation of O_2 on Pt (111) in acidic media. J. Phys. Chem. C. 113, 20657-20665.

Perdew, J.P., Burke, K., Ernzerhof, M., 1996. Generalized gradient approximation made simple. Phys. Rev. Lett. 77, 3865.

Pestana, C.F.M., Guerra, A.C.O., Ferreira, G.B., 2013. Oxidative dehydration of glycerol to acrylic acid over vanadium-impregnated zeolite beta. J. Brazil. Chem. Soc. 24, 100-105.

Shen, Y.H., Li, Y.M., Liu, H.C., 2015. Base-free aerobic oxidation of glycerol on TiO_2-supported bimetallic Au-Pt catalysts. J Energy. Chem. 24, 669-673.

Tran, H.V., Doan, H.A., Chandler, B.D., Grabow, L.C., 2016. Water-assisted oxygen activation during selective oxidation reactions. Curr. Opin. Chem. Eng., 13, 100-108.

Villa, A., Veith, G.M., Prati, L., 2010. Selective oxidation of glycerol under acidic conditions using gold catalysts. Angew. Chem. Int. Edit. 49, 4499-4502.

Wang, F.F., Shao, S., Liu, C.L., Xu, C.L., Yang, R.Z., Dong, W.S., 2015. Selective

oxidation of glycerol over Pt supported on mesoporous carbon nitride in base-free aqueous solution. Chem. Eng. J. 264, 336-343.

Westaway, K.C., 2007. Determining transition state structure using kinetic isotope effects. J. Labelled. Compd. Rad. 50, 989-1005.

Xiao, Y., Greeley, J., Varma, A., Zhao, Z.J., Xiao, G.M, 2016. An experimental and theoretical study of glycerol oxidation to 1, 3-dihydroxyacetone over bimetallic Pt-Bi catalysts. AIChE J. 63, 705-715.

Xu, C.W., Tian, Z.Q., Shen, P.K., Jiang, S.P., 2008. Oxide (CeO_2, NiO, Co_3O_4 and Mn_3O_4)-promoted Pd/C electrocatalysts for alcohol electrooxidation in alkaline media. Electrochim. Aata. 53, 2610-2618.

Zhang, M.Y., Nie, R.F., Wang, L., Shi, J.J., Du, W.C., Hou, Z.Y., 2015. Selective oxidation of glycerol over carbon nanofibers supported Pt catalysts in a base-free aqueous solution. Catal. Commun. 59, 5-9.

Zhou, C.H., Beltramini, J.N., Fan, Y.X., Lu, G.Q., 2008. Chemoselective catalytic conversion of glycerol as a biorenewable source to valuable commodity chemicals. Chem. Soc. Rev. 37, 527-549.

Zope, B.N., Hibbitts, D.D., Neurock, M., Davis, R.J., 2010. Reactivity of the gold/water interface during selective oxidation catalysis. Science. 330, 74-78.